Impurity Transport and Control in ASDEX Upgrade

R. Dux, R. Neu, C.F. Maggi, A.G. Peeters, T. Pütterich, G. Pereverzev, A. Mück, F. Ryter, J. Stober, B.Zaniol† and ASDEX Upgrade team

Max-Planck-Institut für Plasmaphysik, EURATOM Association, D-85748 Garching
† Consorzio RFX, EURATOM Association, Padova, Italy
e-mail: Ralph.Dux@ipp.mpg.de

Abstract Impurity transport parameters of Si and Ne have been determined for H-mode and improved H-mode plasmas with and without central wave heating. The diffusion coefficient D is always anomalous in the edge region and about neoclassical in the centre, when central heating powers are low. Sufficient central wave heating increases the central D and leads also to a flattening of the central density profile. Accumulation of W has been studied in improved H-mode discharges. It strongly depends on the density peaking, and can become severe for purely NBI heated discharges with peaked density profiles, while for flat density profiles, which are achieved with sufficient central wave heating, the W concentrations are flat. Extrapolations of the found impurity behaviour were used to guide a case study of particle transport for the ITER-FEAT inductive operation reference scenario. It suggests sufficient anomalous transport and thus negligible impurity accumulation in the inner plasma region.

1. Introduction

The control of central impurity accumulation by central heating with ECRH or ICRH, which has been developed at ASDEX Upgrade [1], is now a well established experimental control tool. A centrally peaked density profile is accompanied by density peaking of the impurities, which becomes very strong for the high-Z elements like tungsten. This central peaking vanishes when adding a sufficient amount of central wave heating. This valuable tool is especially important in discharge scenarios without sawteeth, e. g. improved H-modes. The present understanding attributes the flattening effect to an increase of the turbulent transport. The temperature profiles in ASDEX Upgrade discharges without internal transport barrier are generally observed to be self similar[2–4]: an increase of central heat deposition profiles thus leads to an increase of the central heat diffusion coefficient χ and anomalous diffusion coefficient for main ion [5,6] and impurities [7]. This increase of anomalous diffusion counteracts the neoclassical inward pinch effects, like the Ware pinch for the main ions, and the impurity inward pinch caused by the main ion density peaking.

This paper describes experimental determinations of the impurity transport coefficients of Si and Ne in H-mode and improved H-mode discharges, where the change of the transport coefficients with the addition of on- and off-axis wave heating was investigated. The transport experiments are complemented by investigations of the effect of central wave heating on the central concentration of C and W in improved H-mode discharges. Finally, the present understanding on central impurity transport is projected to the ITER-FEAT reference scenario for inductive operation using particle transport calculations for different assumptions on anomalous particle transport.

2. Impurity Transport Experiments

In type-I ELMy H-mode discharges, direct measurements of the transport coefficients of silicon were performed using Si laser blow-off (LBO) [7]. The Si density profile evolution was inferred from the signals of two soft X-ray (SXR) cameras. The Si density evolution after LBO is fitted by the numerically calculated solutions of the radial transport equation. The transport induced by sawtooth crashes is treated by assuming a complete flattening of the impurity density inside a mixing radius at the time of the sawtooth crash. Thus, the evaluated impurity diffusion coefficient represents the transport between the sawtooth crashes. The experimental effective heat diffusion coefficient χ_{eff} was evaluated with ASTRA [8]. Deposition profiles of the electron

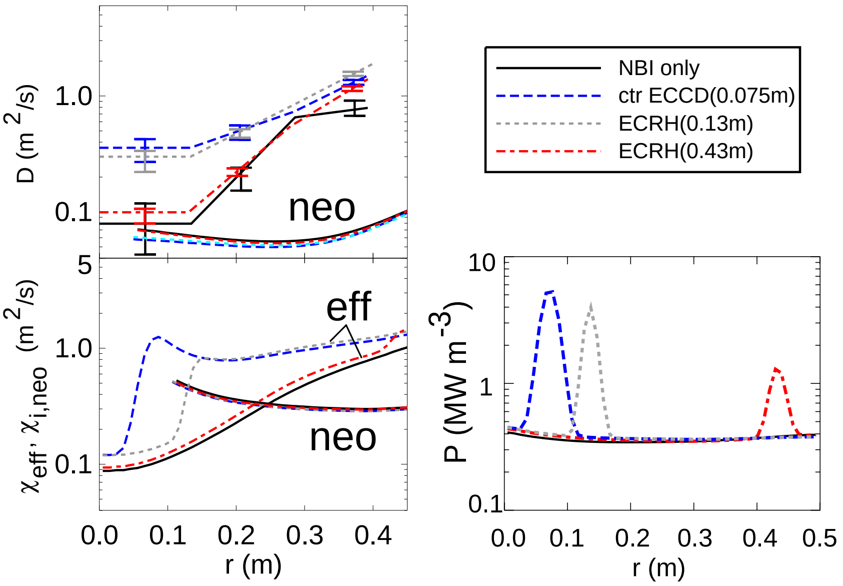

Figure 1: *Measured and neoclassical diffusion coefficient of Si, measured effective and neoclassical ion heat diffusivity, for a series of H-mode discharges at ASDEX Upgrade with NBI heating (P_{NBI}=5 MW) and additional ECR heating at different radial positions r=0.075 m, 0.13 m, and 0.43 m (P_{ECRH}=0.8 MW). The various power deposition profiles are shown in the right graph.*

cyclotron waves were calculated with the TORBEAM code [9], which uses beam tracing techniques [10] to describe propagation and absorption of the beam including diffraction effects. The ECRH profile is approximated by a Gaussian in ASTRA. D_{neo} for Si and $\chi_{i,neo}$ were numerically calculated from standard neoclassical theory [11] using NEOART [12,13] considering a 'typical' impurity composition with 5% He, 1% C , 0.5% O, and 0.1% Si. Neoclassical values are only shown for $r > 2r_{potato}$, where r_{potato} is a simple estimate of the width of the potato orbit passing through the magnetic axis.

Fig.1 shows the results for a series of type-I ELMy H-mode discharges with 5 MW of NBI heating (D$\rightarrow$D$^+$) without/with 0.8 MW of ECRH at different plasma radii. The plasma radius r shall be defined by the volume V enclosed by the flux surface, i. e. $r = \sqrt{V/(2\pi^2 R_{axis})}$. The discharges with NBI only and ECRH at r=0.43 m show a similar radial dependence of D and χ_{eff}. Inside of $r\approx$0.15 m, the Si diffusion coefficient equals the neoclassical value in both cases and χ_{eff} is below $\chi_{i,neo}$. For $r>$0.15 m, D increases with radius and at r=0.4 m, it is about an order of magnitude above D_{neo}. These discharges have also the highest inward pinch parameter v$/D$. There is a drastic change of the transport parameters for the cases with central ECR heating. χ_{eff} rises by up to a factor of 10 for radii greater or equal to the deposition zone, while the local change of χ_{eff} is small at the edge due to the small change of total heating power by ECRH. In the core, also the measured diffusion coefficient of Si increases with additional central ECRH by a factor of 3 to 4.5 to values around D=0.3 m^2/s, which is a factor $\geq$3 above the neoclassical level. In the radial range around r=0.4 m, there is only a minor change between the different heating scenarios.

In another series of H-mode discharges, where the sawteeth were suppressed by 0.8 MW of co-current ECCD at r=0.2 m or 0.8 MW of central counter ECCD, similar results were obtained. The central diffusion coefficient was about a factor of 10 above D_{neo} for central ECCD and approximately equal to D_{neo} with pure NBI heating. In a discharge, which only had central ICR heating with similar maximum power densities in the centre as in the ECR heated cases, a central diffusion coefficients of $D\approx2\times D_{neo}$ was measured, while off-axis ICRH yielded $D\approx D_{neo}$.

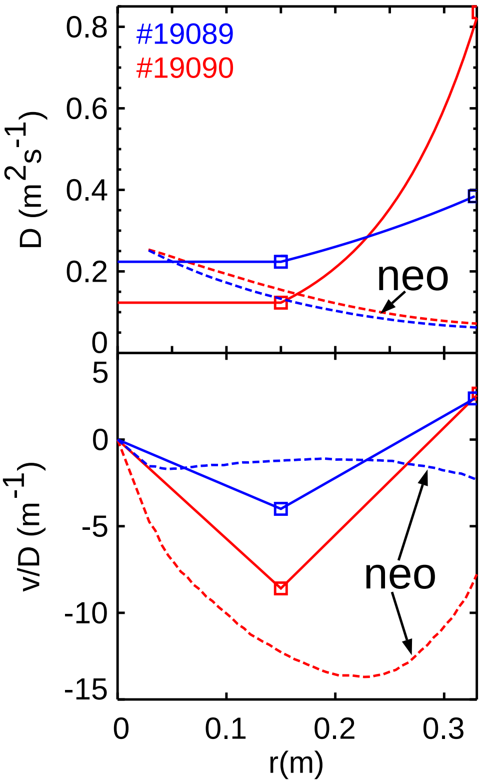

Figure 2: *Measured and neoclassical diffusion coefficient D and drift parameter* v/D *of Ne for two improved H-mode discharges at ASDEX Upgrade with NBI heating (*P_{NBI}*=7 MW) and additional ICR heating of* P_{ICRH}*=3 MW in #19090 and* P_{ICRH}*=5 MW in #19089.*

In the plasmas of all these series, where anomalous transport was dominant, the measured inward pinch parameter v/D was low [7].

The effect of central ICRH on impurity transport was also studied for Ne in improved H-mode discharges [14]. Densities of fully ionised Ne were obtained from charge exchange recombination spectroscopy (CXRS). For a Ne puff of 20 ms duration, the measured density evolution on the 6 innermost channels of the CXRS diagnostic with r/a below $\approx$0.5 were fitted to obtain the transport coefficients. Fig.2 shows the results for two deuterium discharges at I_p=1 MA, q_{95}=3.8, triangularity δ=0.23 and line averaged densities $\bar{n}_e \approx 5.5\times10^{19}\mathrm{m}^{-3}$ which equals 0.42 of the Greenwald density. Heating powers were $P_{\mathrm{NBI}} \approx 6.5$ MW and $P_{\mathrm{ICRH}} \approx 5$ MW in #19089 and $P_{\mathrm{NBI}} \approx 7$ MW and $P_{\mathrm{ICRH}} \approx 3$ MW in #19090. In the discharge with lower P_{ICRH} (#19090) the fitted central diffusion coefficient is about a factor of 2 lower than in #19089. In #19090, the impurity transport is more convective, i. e. higher absolute values of the drift parameter v/D are measured. The drift velocities are negative, denoting and inwardly directed drift. The measurements are compared with neoclassical transport coefficients as calculated with NEOART. The neoclassical diffusion coefficient is very similar in both discharges, however, there is a much stronger neoclassical inward pinch parameter v_{neo}/D_{neo} in #19090. This difference in the neoclassical inward pinch reflects the differences in the density profiles. For #19090, the density profile is peaked within $r/a \approx$0.5 and $n_e(0) = 2n_e(r = a/2)$, while it is only $n_e(0) = 1.3n_e(r = a/2)$ for #19089.

For this pair of discharges, a strong difference was also found for the tungsten behaviour. The tungsten concentrations are derived from two spectroscopic measurements. Towards the plasma edge, the intensity of the W quasi-continuum around 5 nm, which is emitted from ions around W^{28+} [15], delivers the concentration $c_{\mathrm{W}}^{1\mathrm{keV}}$ for the plama radius with T_e of about 1 keV, and

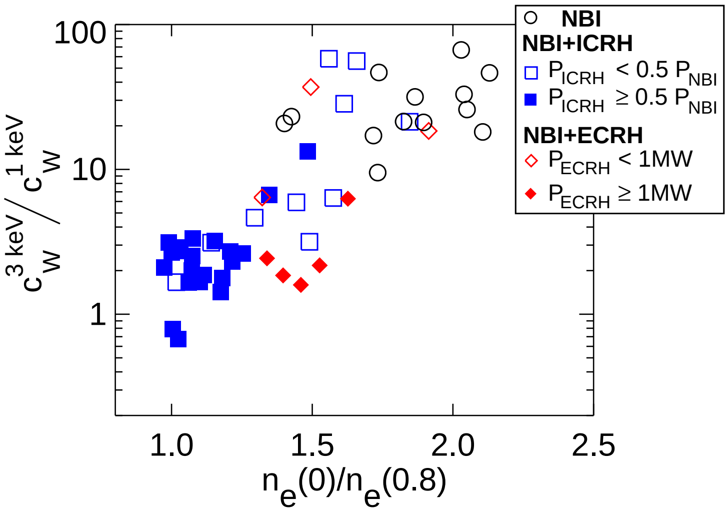

Figure 3: *Ratio of central and edge tungsten concentration versus density peaking for improved H-mode discharges.*

the intensity on a Ni-like (W^{46+}) line at λ=0.793 nm [16,17] is used to deduce the central concentration c_W^{3keV} at $T_e \approx$3 keV. For #19089, both concentrations are low at c_W^{1keV}=8×10^{-6} and c_W^{3keV}=5×10^{-5}, while central tungsten accumulation is observed in #19090 with c_W^{1keV}=7×10^{-6} and c_W^{3keV}=4×10^{-4}. For #19090, the values are taken just before the Ne puff, sine it leads to a reduction of central T_e below 2.5 keV, such that central line emission from W^{46+} becomes low, while the emission region of the quasi-continuum is considerably shifted towards the centre. It should be mentioned that the electron density peaking is not caused by the W accumulation, and the electrons from W are still below 2% in #19090.

The Z-dependence of the peaking amplitudes of Ne and W is quite remarkable and is in accordance with earlier observations of the Z-dependence of impurity accumulation in H-modes and internal transport barrier discharges [18–20]. Taking the measured v$/D$-profiles from Ne, one can derive the peaking of the steady state Ne concentration profile, which yields $c_{Ne}(0)/c_{Ne}(r=a/2) \approx 1.7$ for #19089 and $c_{Ne}(0)/c_{Ne}(r=a/2) \approx 3.5$ for #19090. For W, however, the concentration ratios are $c_W^{3keV}/c_W^{1keV} \approx$6 for #19089 and $c_W^{3keV}/c_W^{1keV} \approx$60 for #19090.

3. Impurity Control in Improved H-mode

The use of central wave heating as a control tool to flatten the main ion density profile and to avoid tungsten accumulation has previously been shown for dedicated improved H-mode discharges [21,22]. Additionaly, a strong influence of central wave heating on the central impurity peaking became evident from an anlysis of the central radiation profile [21]. In Fig.3, the sensitivity of tungsten accumulation on the density peaking is shown for a broader data base of improved H-mode discharges, containing purely NBI heated plasmas (circles) as well as discharges with additional ECR- (diamonds) and ICR-heating (squares). Filled squares are used for plasmas with $P_{\mathrm{ICRH}} \geq 0.5 P_{\mathrm{NBI}}$ and filled diamonds for cases with $P_{\mathrm{ECRH}} \geq 1$ MW. The ratio of the two spectroscopically determined tungsten concentrations c_W^{3keV}/c_W^{1keV} covers a wide range from about 1 to almost 100, with a very strong dependence on the density peaking, which is given by the ratio of density on axis $n_e(0)$ and density $n_e(0.8)$ at poloidal flux label ρ_{pol}=0.8. Highest density peaking and strong tungsten accumulation is found for purely NBI heated discharges or discharges with lower amount of wave heating, while the other extreme case of flat density and flat tungsten concentration profiles occurs for discharges with sufficient wave heating. Additionaly, carbon concentration profiles have been measured in improved H-modes with

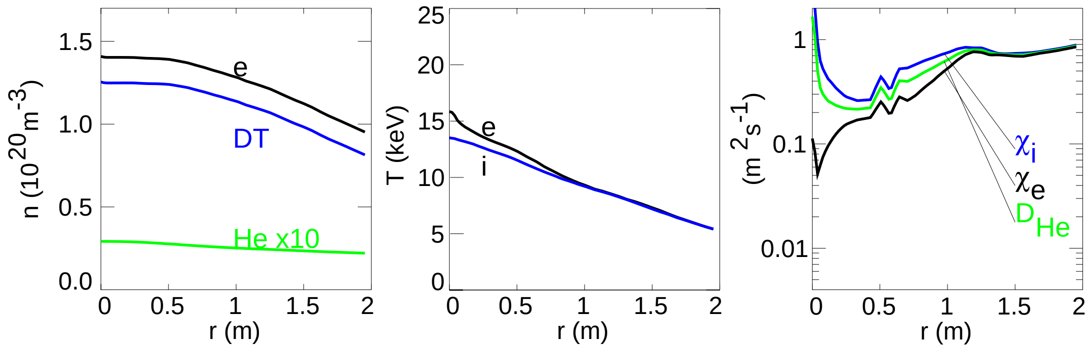

Figure 4: *Predictions for density and temperature profiles in ITER-FEAT for the* $Q = 10$ *reference scenario with inductive operation using GLF23 [8].*

CXRS [14]. Here, the effects are of course less dramatic compared to tungsten but show a similar trend with density peaking. Central values of c_{C}=3% are reached in cases with peaked density profiles which are reduced to the 1% level for flat density profiles with sufficient central heating.

4. ITER Predictions

The findings of the above sections are promising with regards to impurity transport in a burning reactor, since α-heating provides a centrally peaked power deposition profile. The expected α-heating power densities of about 1 MWm^{-3} are considerably lower than the few MWm^{-3}, which were achieved with the central wave heating used in the reported experiments (see Fig. 1). However, due to the increased size of the reactor by a factor of about 5, heat flux densities will be of comparable size at about 1/10 of the minor radius. It remains open, whether the temperature gradients in the reactor will become critical at a sufficiently small radius to drive the central energy and particle transport anomalous. If this assumption holds, then He ash removal from the core would be sufficient and the equilibrium concentration profiles of impurities originating from plasma facing components, which solely depend on the drift parameter v/D, would be flat. The main ion density profile might even be peaked due to the anomalous inward pinch, which has been shown to become important for low collisionality plasmas [23]. However, as long as turbulent transport prevails, impurity accumulation is not expected to occur and was never detected in plasmas with dominant anomalous transport.

This is illustrated with impurity transport calculations for the ITER-FEAT reference scenario for inductive operation. The starting point is a calculation of heat and particle transport using the ASTRA code [8,24]. The main parameters are: R =6.2 m, a=2.4 m, B_T=5.3 T, I_p=15 MA, U_{loop}=0.075 V, P_{NBI}=40 MW, P_{fus}=400 MW. The anomalous fluxes of electrons and heat are calculated with the GLF23 code [25], which is based on ITG/TEM physics. GLF23 does not treat impurity transport and only diffusive transport of Helium is considered, with $D_{an} = (\chi_i + \chi_e)/2$. Dilution and radiative losses by Be(2%) and Ar(0.12%) are included using fixed concentrations. In Fig.4, the resulting profiles of n_e, $n_{DT} = n_D + n_T$, n_{He}, T_e, and T_i are shown with the anomalous heat diffusion coefficients χ_i and χ_e. There is an inwardly directed particle drift, which leads to the peaking of n_e and n_{DT}. The transport coefficients are not delivered by GLF23, which just returns radial fluxes.

In the next step, impurity transport is considered for He, Be, Ar and W inside of r/a=0.8. All elements are given a fixed edge concentration: $c_{\mathrm{He}} = 2.3\%$, $c_{\mathrm{Be}} = 2\%$, $c_{\mathrm{Ar}} = 0.1\%$, and $c_{\mathrm{W}} = 0.001\%$. The anomalous diffusion coefficient is given a very simple shape with constant levels for $r < 0.7$ m as well as for $r > 1.2$ m, which are linearly interpolated for $0.7\,\mathrm{m} < r < 1.2$ m, and at the beginning, the inner and outer levels are chosen to be at $D_{an,in}$ =0.2 m^2/s and

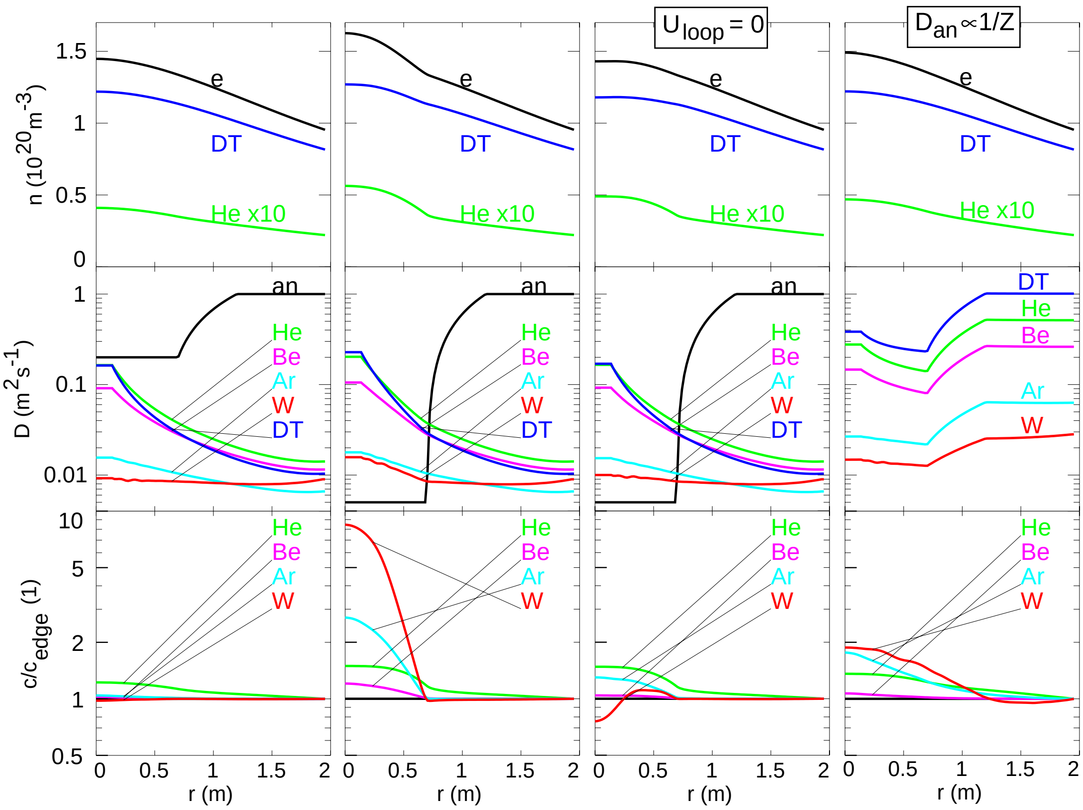

Figure 5: *Simulated density profiles of D+T, He, Be, Ar and W in ITER-FEAT for the* $Q = 10$ *reference scenario with inductive operation using different assumptions about anomalous impurity transport. 1st column: dominant anomalous transport in centre as in Fig.4 with* D_{an} *and* v_{an} *equal for all ions. 2nd column: dominant neoclassical transport in centre. 3rd column: dominant neoclassical transport in centre and Ware pinch switched off. 4th column:* D_{an} *and* v_{an} *scale with* $1/Z$*. The second row gives anomalous and neoclassical diffusion coefficients for column 1-3, and total diffusion coefficients for colum 4.*

$D_{an,out} = 1$ m^2/s, which approximately reflects the GLF23 profile of $(\chi_i + \chi_e)/2$ from Fig.4. The anomalous drift velocity v_{an} is adopted to fit the n_{DT} profile, which was calculated by GLF23. D_{an} and v_{an} are assumed to be equal for all ions. D_{neo} and v_{neo} for the 6 components D, T, He, Be, Ar, and W is calculated with NEOART. The transport of all ions is calculated, n_e follows from the condition of quasi-neutrality, and the profiles of T_e, T_i, and consequently also of the fusion reaction coefficient are kept fixed.

Fig.5 shows the equilibrium density profiles, the diffusion coefficients, and the radial shape of the impurity concentrations normalised to their edge value for four different cases. In the first column, the D_{an} levels were taken at about $(\chi_i + \chi_e)/2$ as given by GLF23. He is slightly more peaked compared to Fig.4, since the anomalous drift has been taken into account. D_{neo} is below D_{an} for all species and all radii, and neoclassical transport has almost no influence. Since D_{an} and v_{an} are equal for all species, the concentrations of Be, Ar and W are radially constant. The profiles of the second column are calculated for the case of a low anomalous diffusion coefficient in the inner region, i. e. lower than the neoclassical value of all species. It represents the worst case estimate with respect to He removal and neoclassical impurity accumulation. For He, the additional peaking is predominantly caused by the central fusion source at the lower diffusion coefficient, which requires a larger gradient to maintain the radial flux. For the other impurities, the central peak in the concentration is caused by the neoclassical inward pinch, and rises with the impurity charge. D and T are still peaked in the inner region, even though the anomalous inward pinch plays no role. This is due to the neoclassical Ware pinch as is demonstrated in the third column. Here, the Ware pinch was switched off by artifically setting U_{loop} to zero. The main ion peaking in the neoclassically dominated radial range disappears, the drive for the neoclassical peaking of Be, Ar and W is lost, and their concentration profiles are almost flat. Only for He, the profile is nearly unchanged, since here the peaking was mainly caused by the central fusion source. A strong dependence of turbulent diffusion on impurity mass or charge has not been found experimentally. Nevertheless, the influence of an anomalous diffusion coefficient, which decreases with impurity charge is demonstrated in the 4th column to include a more unfavourable case for the accumulation of high-Z elements. Here, only the ratio v_{an}/D_{an} is taken not to depend on impurity charge. For D and T, the same levels as in the first column are chosen, and for the other impurities D_{an} shall be proportional to Z^{-1}. Here, D, T, and Be are similarly peaked due to v_{an}, while the high-Z elements feel the neoclassical pinch, which is driven by the peaked low-Z elements. The He profile is not strongly influenced.

As long as turbulent transport is dominant, no impurity accumulation is expected from present experimental experience, which tells, that v_{an}/D_{an} does not increase significantly with ion charge. Only for very low anomalous transport, central accumulation of high-Z elements is found, which is driven by the peaking of the main ion species due to the Ware pinch. Since the loop voltage and consequently the Ware pinch are quite low in ITER-FEAT, even a low amount of anomalous diffusion is sufficient to control the neoclassical peaking. The GLF23 results for inductive operation without a central transport barrier suggest sufficient anomalous transport, even in the inner plasma region.

References

[1] NEU, R. et al., Plasma Phys. Controlled Fusion **44** (2002) 811.
[2] SUTTROP, W. et al., Plasma Phys. Controlled Fusion **39** (1997) 2051.
[3] STOBER, J. et al., Plasma Phys. Controlled Fusion **42** (2000) A211.
[4] TARDINI, G. et al., Nucl. Fusion **42** (2002) 258.
[5] STOBER, J. et al., Nucl. Fusion **41** (2001) 1535.
[6] STOBER, J. et al., Nucl. Fusion **43** (2003) 1265.
[7] DUX, R. et al., Plasma Phys. Controlled Fusion **45** (2003) 1815.
[8] PEREVERZEV, G. et al., 'ASTRA Automated System for Transport Analysis in a Tokamak', IPP-5/98, Max-Planck-Institut für Plasmaphysik, Garching, Germany (2002).
[9] POLI, E. et al., Computer Phys. Comm. **136** (2001) 90.
[10] PEREVERZEV, G. V., Phys. Plasmas **8** (2001) 3664.
[11] HIRSHMAN, S. P. et al., Nucl. Fusion **21** (1981) 1079.
[12] PEETERS, A. G., Phys. Plasmas **7** (2000) 268.
[13] DUX, R. et al., Nucl. Fusion **40** (2000) 1721.
[14] MAGGI, C. F. et al., Impurity control in improved h-mode scenarios in ASDEX Upgrade, in *Europhysics Conference Abstracts (CD-ROM, Proc. of the 31st EPS Conference on Controlled Fusion and Plasma Physics, London, 2004)*, volume 28B, pages P–4.119, Geneva, 2004, EPS.
[15] ASMUSSEN, K. et al., Nucl. Fusion **38** (1998) 967.
[16] NEU, R. et al., Physica Scripta **T92** (2001) 307.
[17] NEU, R. et al., Tungsten: An option for divertor and main chamber plasma facing components in future fusion devices, in *this conference*.
[18] DUX, R. et al., Nucl. Fusion **44** (2004) 260.
[19] DUX, R. et al., J. Nucl. Mater. **313-316** (2003) 1155.
[20] DUX, R. et al., Nucl. Fusion **39** (1999) 1509.
[21] NEU, R. et al., J. Nucl. Mater. **313–316** (2003) 118.
[22] DUX, R. et al., Fusion Tech. **44** (2003) 708.
[23] ANGIONI, C. et al., Phys. Rev. Lett. **90** (2003) 205003.

[24] PEREVERZEV, G. V. et al., Predictive simulation of ITER performance with theory-based transport models, in *Europhysics Conference Abstracts (CD-ROM, Proc. of the 30th EPS Conference on Controlled Fusion and Plasma Physics, St. Petersburg, 2003)*, edited by KOCH, R. et al., volume 27A, pages P–3.138, Geneva, 2003, EPS.

[25] WALTZ, R. E. et al., Phys. Plasmas **4** (1997) 2482.